Published in final edited form as:
Biochemistry. 2012 December 21; 51(51): 10236–10243. doi:10.1021/bi301224b.

Magnesium Induced Nucleophile Activation in the Guanylyltransferase mRNA Capping Enzyme

Robert V. Swift[1], **Chau D. Ong**[2], and **Rommie E. Amaro**[1,*]

[1]Department of Chemistry and Biochemistry, University of California, San Diego, La Jolla, California, 92039

[2]Lake Erie College of Osteopathic Medicine, 5000 Lakewood Ranch Blvd. Brandenton, Florida 34211

Abstract

The messenger RNA guanylyltransferase, or mRNA capping enzyme, co-transcriptionally caps the 5′-end of nascent mRNA with GMP during the second in a set of three enzymatic reactions that result in the formation of an N7-methyl guanosine cap during mRNA maturation. The mRNA capping enzyme is characterized, in part, by a conserved lysine nucleophile that attacks the alpha-phosphorous atom of GTP, forming a lysine-GMP intermediate. Experiments have firmly established that magnesium is required for efficient intermediate formation, but have provided little insight into the requirement's molecular origins. Using empirical and thermodynamic integration pKa estimates, along with conventional MD simulations, we show that magnesium binding likely activates the lysine nucleophile by increasing its acidity and by biasing the deprotonated nucleophile into conformations conducive to intermediate formation. These results provide additional functional understanding of an important enzyme in the mRNA transcript life cycle and allow functional analogies to be drawn that affect our understanding of the metal dependence of related superfamily members.

Introduction

During transcription, within the nuclei of eukaryotic cells, GTP-dependent mRNA capping enzymes, members of the nucleotidyltransferase superfamily, participate in the addition of an N7-methyl-GMP cap to the 5′-end of nascent mRNA, a critical modification that plays several essential roles in the functional cycle of mRNA. Cap recognition is essential in mRNA splicing, transcript stability, nuclear export, and ribosomal translation initiation (1–3). Due to its fundamental role in many of the events responsible for the normal flow of biologic information, the presence of an mRNA cap is essential in all eukaryotic cell types examined thus far (4–9). Cap formation occurs by a set of three sequential enzymatic reactions, the mRNA capping enzyme carries out the second of these. During the first step, the 5′-phosphate is hydrolyzed from nascent mRNA by a triphosphatase. In the second step, the resulting 5′-diphosphate end is guanylated by a guanylyl transferase, or mRNA capping enzyme. Finally, during the third step, the N-7 nitrogen atom is methylated by a methyltransferase. GTP dependent-mRNA capping enzymes belong to a larger superfamily of enzymes called the nucleotidyltransferase superfamily, whose members also include

*Corresponding author contact information: Telephone: (858) 534-9629, Fax: (858) 534-9645, ramaro@ucsd.edu.

Supporting Information Available

Supporting information includes plots of the distance and angle time series used to construct figures 4A and 5A, as well as corresponding one-dimensional histograms. This material is available free of charge via the Internet at http://pubs.acs.org.

ATP- and NAD^+-dependent DNA ligases, and ATP-dependent RNA ligases (10). Members share common structural features and catalyze reactions following similar mechanisms (10).

Biochemical (11, 12), structural (13), and kinetic (14) studies independently demonstrated that a magnesium ion is required for the capping enzyme to efficiently catalyze GMP transfer. Following GTP binding, the first chemical step of the reaction occurs when a conserved lysine nucleophile attacks the alpha-phosphorus atom of GTP, displacing pyrophosphate and forming a lysine-GMP intermediate (figure 1). Following the release of pyrophosphate, nascent mRNA binds to the intermediate, and GMP is transferred from the lysine nucleophile to the mRNA 5′-phosphate during the second and final chemical step of the reaction (figure 1). Although magnesium binding is a known prerequisite of both chemical steps (14), the molecular origins of the requirement are ambiguous, and several possible explanations may suffice (15). For example, assuming the first chemical step is an associative in-line attack (16, 17), the divalent magnesium cation may stabilize the negative charge present in the pentavalent transition state. Magnesium binding may also influence active-site geometry, optimally orienting the lysine nucleophile and pyrophosphate leaving group for lysine-GMP intermediate formation. Still another possibility is that magnesium binding increases the acidity of the lysine nucleophile, effectively raising the concentration of reactive enzyme. This is not an exhaustive list, and the possibilities given may all enhance catalysis to varying extents.

In this work, we explore the influence of magnesium binding on activating the lysine nucleophile during the first chemical step in the mRNA capping reaction. We examine how magnesium binding may affect lysine nucleophile acidity and influence the conformational distribution of the deprotonated lysine nucleophile. Specifically, empirical pKa estimates and thermodynamic integration (TI) were used to estimate changes in lysine nucleophile acidity that may occur on magnesium binding. Additionally, conventional molecular dynamics (MD) simulations were carried out in the presence and absence of magnesium to determine the influence of magnesium binding on the distance between the nucleophile and electrophile, as well as the angle formed by the nucleophile, electrophile and leaving group. Throughout this work, structures from the *Paramecium bursaria Chlorella* virus 1 (PBCV-1), the smallest functional mRNA capping enzyme known (11, 13), were used.

Materials and Methods

Empirical pKa estimates

PROPKA3 (18–21) was used to carry out empirical pK_a estimates. PROPKA3 benefits from explicitly incorporating the columbic interactions that arise from mutually titrating residues *via* the Tanford-Roxby scheme (20, 22), but it suffers from implicit estimations of the conformational reorganization that alter a titrating residues microenvironment and affect its pK_a (23). Consequently, titrations in which conformational reorganization plays a significant role may be inaccurately estimated. To carry out the PROPKA3 estimates, a model of the magnesium-bound GTP complex was first constructed from chain B of PDBID 1ckm and chain B of PDBID 1ckn (13). Using the RMSD trajectory tool in VMD (24), the two chains were aligned by their alpha carbon atoms. Following alignment, the magnesium was positioned in chain B of PDBID 1ckm to overlap with the location of manganese from chain B of PDBID 1ckn. This model, along with chain B of PDB ID 1ckm, was submitted to the PROPKA server, and the results were used to estimate the effects of magnesium binding on the acidity of the lysine nucleophile.

Thermodynamic Integration (TI)

TI (25, 26), which relies on MD simulations (26), more adequately captures the conformational reorganization that may occur upon residue titration. However, as MD simulations rely on classical mechanics to propagate system dynamics, traditionally, only a single residue of interest may change protonation state, while the protonation states of other residues remain fixed (27–29). Hence, despite more accurately modeling conformational affects, TI suffers from complete neglect of coupled titration. While neither PROPKA nor TI perfectly capture the physics of multi-site titration, and neither is likely to give a completely accurate answer, their trends should provide a qualitatively reasonable understanding of the effects of magnesium binding on the acidity of the lysine nucleophile. Below, we develop thermodynamic integration in greater detail.

The change of lysine nucleophile acidity upon magnesium binding is measured by the extent of proton dissociation in the presence and absence of bound magnesium, as described by the two reactions in figure 2. The extent of proton dissociation in each reaction is measured by the reaction equilibrium constant, K_a, which is related to the free energy change, ΔG:

$$\Delta G = -\frac{1}{\beta}\ln(K_a) \quad 1$$

In equation 1, $\beta^{-1}=RT$, with R the universal gas constant and T the temperature. Using equation 1, the pK_a, defined as the negative log of the equilibrium constant, is expressed:

$$pK_a = \frac{\beta}{\log(e)}\Delta G \quad 2$$

With equation 2, the extent of nucleophile deprotonation upon magnesium binding, relative to the extent of deprotonation in the absence of magnesium, can be formulated in terms of the double free energy difference, $\Delta\Delta G = \Delta G(KH^+ \cdot Mg^{2+}) - \Delta G(KH^+)$, which is given by the thermodynamic cycle in figure 2:

$$\Delta pK_a = \frac{\beta}{\log(e)}\Delta\Delta G \quad 3$$

In equation 3, the pK_a difference, ΔpK_a, is given, $\Delta pK_a = pK_a(KH^+ \cdot Mg^{2+}) - pK_a(KH^+)$.

Thermodynamic integration (TI) was used to estimate the double free energy difference in equation 3. In TI, the potential energy is expressed as a function of a coupling parameter, λ, whose value ranges from zero to one between endpoints. Assuming negligible volume changes along the transformation pathway, NPT and NVT results are equivalent, and the free energy change between pathway endpoints is expressed as:

$$\Delta G = \int_{\lambda=0}^{\lambda=1}\left\langle\frac{\partial U}{\partial\lambda}\right\rangle_\lambda d\lambda \quad 4$$

Each free energy difference was calculated in three steps. First, the side chain of the positively charged, protonated lysine nucleophile was electrostatically decoupled from its environment by scaling the atomic partial charges to zero. Next, by scaling the van der Waals potential to zero, the non-bonded interactions between one of the side chain amine protons and the surroundings was annihilated. Last, the atomic partial charges of the

deprotonated lysine side chain were scaled from zero to one, electrostatically coupling the side chain and surroundings. The integrand of equation 4 was estimated at nineteen equally spaced λ values and numerically integrated using the trapezoidal rule for each transformation.

Integrand averages in equation 4 were estimated by MD simulations performed with the sander program in version ten of the Amber simulation suite (30). The GTP bound system was constructed from chain B of PDBID 1ckm. The magnesium-bound GTP complex was built using the model described in the *Empirical pKa estimates* section, above. With the exception of the lysine nucleophile, K82, which was protonated in both systems, protonation states were predicted using the PROPKA server. The Amber 99 force field (31), with the Stony Brook corrections (32), was used to describe the protein, while the Meagher-Carlson parameters were used to describe GTP (33). Magnesium was represented by the Oelschlaeger-Warshel parameters, which delocalize charge over a central atom and six cationic dummy-atoms, providing a more accurate depiction of divalent metal-ion electrostatics and geometry (34). While the presence of divalent magnesium may result in some charge redistribution of surrounding residues, we assumed the affects would be modest and neglected them. Ultimately, the validity of this assumption is subjective. However, as our results, discussed below, provide a reasonable interpretation of macroscopic observables consistent with generally accepted principles of enzyme mechanism, neglecting charge redistribution effects is a sensible, simplifying assumption for this study. Each system was immersed in a pre-equilibrated box of TIP3P water (35) that provided a 10Å buffer between the longest protein dimension and the water box edge along the x-, y-, and z-axes. The systems were brought to electric neutrality by the addition of sodium ions. At each λ value, systems were minimized for 1000 steps using the steepest descent algorithm. To equilibrate system density, 100ps of simulation at 1atm and 300K were conducted. Averaging followed and was performed over 2.25ns of simulation in the NVT ensemble at 300K; data points were sampled every 50ps. A 1fs time step was used in both ensembles. Temperature was controlled using a Langevin thermostat (36) with a collision frequency of $5ps^{-1}$, and pressure was controlled with a Berendsen barostat (37). An 8Å non-bonded cutoff was used, and long-range electrostatics were evaluated by the PME method (38) with default grid spacing. Charge coupling contributions due to self-interactions between periodic images are essentially identical along the legs of the thermodynamic cycle and can be neglected (39). To prevent the so-called end-point catastrophe (40), a soft-core potential (41) was used to perform simulations that scaled the van der Waals potential. All Standard errors were calculated using distributions generated by bootstrap re-sampling the data, with replacement (42).

Conventional MD simulations

To probe the effects of magnesium binding on activesite geometry, additional GTP-bound simulations were constructed both with and without bound magnesium. In all simulations, the lysine nucleophile was modeled in a deprotonated, neutrally charged state. Each model was immersed in an explicit water box, counter ions were added, and force field parameters were assigned as described in the *Thermodynamic Integration (TI)* section. Simulations were conducted identically for both models. Following 1000 steps of steepest descent energy minimization, 1 ns of equilibration was carried out at 1atm and 300K before conducting 50ns of NVT simulation at 300K. Temperature, pressure, non-bonded cutoffs, and long-range electrostatics were treated as described in the *Thermodynamic Integration (TI)* section. In both ensembles, a 2fs time step was used; bond lengths between hydrogen and heavy atoms were constrained using the SHAKE algorithm (43).

Results

Magnesium induced pK_a shift

The acidity change of the lysine nucleophile, K82, was estimated by calculating the pK_a shift upon magnesium binding using PROPKA and thermodynamic integration (TI). PROPKA is a rapid empirical approach that utilizes a single structure but accounts for co-titrating residues, while TI approximates ensemble averages using MD simulations but neglects co-titration. Though neither is expected to be completely accurate, the trends provide qualitative insight into the effects of magnesium binding on lysine nucleophile acidity. PROPKA estimates were evaluated using a GTP-bound crystal of the PBCV-1 mRNA capping enzyme, with and without a bound magnesium ion, whose position was modeled. The position was chosen to overlap with a manganese ion, which was observed in an enzyme-GMP intermediate formed by soaking the GTP-bound crystal in a solution of manganese chloride; the choice is reasonable because of the high degree of structural conservation between the lysine-GMP intermediate and the GTP bound crystal structures (13). Similarly, TI-MD simulations were conducted on the GTP-bound structures, with and without the modeled magnesium ion.

PROPKA predicts that magnesium binding facilitates K82 deprotonation. In the absence of bound magnesium, the predicted K82 pK_a is 14.51. Upon introducing magnesium to the GTP-bound crystal structure, the predicted pK_a value decreases by 6.6 units to 7.89, indicating the predicted fraction of K82 in the deprotonated state increases by over six orders of magnitude (table 1).

Similarly, TI predicts that magnesium binding facilitates K82 deprotonation. The time series of the double free energy change, $\Delta\Delta G$, which was determined by subtracting the free energy change of deprotonating K82 in the GTP-bound state from the free energy change of deprotonating K82 in the GTP-magnesium-bound state, is reported in figure 3. The double free energy change reaches a plateau after roughly 1ns, taking a final value of −5.7+/−0.5 kcal/mol after 2.25ns. The negative double free energy change predicts that it is thermodynamically more favorably for K82 to release a proton following magnesium binding. Consistent with these predictions, the pK_a of K82 is expected to decrease by 4.2+/−0.3 units after magnesium binds (table 1). The increased acidity would cause the deprotonated fraction of K82 to increase by over four orders of magnitude, a result consistent with the PROPKA estimates.

Magnesium influences active-site geometry

The putative effects of magnesium binding on the relative position and orientation of the lysine nucleophile and pyrophosphate leaving group were assessed by two 50ns MD simulations of the GTP-bound and GTP-magnesium-bound states. The magnesium position was modeled as described in the *Magnesium induced pK_a shift* section. In both simulations, K82 was represented in the deprotonated, or neutral charge state, which is expected to mimic the state that reacts with the alpha-phosphorous atom of GTP. The relative position between the lysine nucleophile and alpha-phosphorous electrophile was determined by measuring the distance between the NZ nitrogen atom of K82 and the PA phosphorus atom of GTP (figure 4B). Similarly, the relative orientation of the nucleophile and pyrophosphate leaving group was determined by measuring the angle formed between the NZ nucleophile atom of K82, the PA electrophile atom of GTP, and the O3A oxygen atom of GTP, the first atom of the pyrophosphate leaving group (figure 4B).

Magnesium binding is predicted to shorten the distance between the nucleophile and electrophile and increase the angle formed by the nucleophile, electrophile, and leaving group. Two-dimensional probability distribution functions (PDFs) that report the probability

of a given distance and angle occurring simultaneously are shown in figures 4A and 5A for the magnesium unbound and magnesium bound simulations, respectively; the time series from which these results were derived, and the corresponding one-dimensional histogram distributions, are shown in the supplementary material.

Figure 4A shows that in the absence of magnesium, the lysine nucleophile predominantly samples two states, one with an average nucleophile-electrophile separation of 4.5Å that takes on values as small as 3.2Å (labeled S1 in figure 4A), the other with an average separation of 6.7Å with values as large as 9.7Å (labeled S2 in figure 4A). In both states, the angle formed between the nucleophile, electrophile, and leaving group is approximately normally distributed, with an average of 141° (figure 4A). In the state with the smaller nucleophile-electrophile separation, S1, the K82 side chain nitrogen atom interacts with the O5′ oxygen atom of GTP (figure 4B). The state with greater nucleophile-electrophile separation, S2, is formed when the K82 side chain moves away from GTP, likely due to electrostatic repulsion, into a pocket formed by the K234, K236, D213, and I216 side chains (figure 4C). In contrast, figure 5A shows that upon magnesium binding, the lysine nucleophile occupies predominantly one state characterized by an average nucleophile-electrophile separation of 3.5Å that takes values as short as 2.9Å and as long as 4.7Å (figure 5A). The angle formed between the nucleophile, electrophile and leaving group is roughly normally distributed with an average of 160°, though angles up to 179.8° occur (figure 5A). This state is stabilized by electrostatic interactions between the negatively charged K82 side chain nitrogen atom and the divalent magnesium cation (figure 5B).

Discussion

Structural, biochemical, and kinetic reports firmly established that magnesium is required for the mRNA capping enzyme to efficiently catalyze lysine-GMP intermediate formation but have provided little insight into the requirement's molecular origins. The computational results presented in this work strongly implicate magnesium in lysine nucleophile activation, facilitating the formation of the lysine-GMP intermediate (figure 1). Magnesium activation is predicted to occur by increasing nucleophile acidity and by biasing the deprotonated nucleophile in conformations conducive to intermediate formation. These results provide additional functional understanding of an important enzyme in the mRNA transcript life cycle and allow functional analogies to be drawn that affect our understanding of the metal dependence of related superfamily members, points we discuss in greater detail below.

Magnesium binding activates the lysine nucleophile, in part, by increasing the fraction of the nucleophile in the deprotonated, reactive state. This result is readily understood in terms of electrostatic arguments and is consistent with both pK_a prediction methods employed. Prior to magnesium binding, a significant fraction of the lysine nucleophile is likely protonated, in an unreactive, metastable state. In this state, elucidated by x-ray crystallography (13), the lysine lacks a reactive electron pair and is positively charged, creating favorable interactions with the nearby, negatively charged GTP triphosphate tail. Magnesium is predicted to bind within 4Å of the lysine nucleophile, resulting in an electrostatically unfavorable interaction that can be mitigated by lysine deprotonation, consistent with the predicted downward pK_a shifts (table 1). Deprotonation exposes an electron pair and, assuming the deprotonated nucleophile obtains a reactive conformation, allows reaction with the alpha phosphorous electrophile, leading to formation of the lysine-GMP intermediate. Thus, by increasing the concentration of the deprotonated nucleophile, magnesium increases the concentration of enzyme that is able to form the lysine-GMP intermediate.

Following deprotonation, magnesium increases the chances that the nucleophile will obtain a reactive conformation, further facilitating lysine-GMP intermediate formation. Phosphoryl

transfer reactions are known to follow three distinct pathways: dissociative, concerted, or addition-elimination (16). In all three pathways, the approaching nucleophile is oriented in-line with the leaving group, and the angle formed between the nucleophile, electrophile and leaving group is 180°. When lysine deprotonation occurs in the absence of magnesium, the simulation results presented here indicate that the deprotonated nucleophile will seldom be both proximal to the electrophile and in-line with the leaving group. For example, in the absence of magnesium, the nucleophile frequently moved to an unreactive distance, away from the electrophile, into an adjacent active site pocket (figures 4A & 4C). This rearrangement is likely due to the electrostatic repulsion between the nucleophile and the GTP alpha-phosphate oxygen atoms. On occasions when the deprotonated lysine nucleophile approached the electrophile, it shifted below the reactive, in-line position, to a position near the O5′ GTP oxygen atom (figure 4C), also likely because of electrostatic repulsion. So, although proximal-in-line conformations conducive to intermediate formation occurred, these conformations were rarely sampled. This is apparent in the diffuse distance-angle distribution, which is sparsely populated for distances less than 3.5Å and angles near 180° (figure 5A). These reactive conformations are made more rare by the smaller fraction of deprotonated lysine-nucleophile expected in the absence of magnesium. Consequently, the chances of lysine-intermediate formation occurring in the absence of magnesium are small, consistent with the available experimental data. In contrast, when lysine deprotonation occurs when magnesium is bound, the deprotonated nucleophile spends more time proximal to the electrophile and in-line with the leaving group, conformations conducive to lysine-GMP intermediate formation. For example, likely because attractive electrostatic interactions between the nucleophile and the divalent magnesium ion offset repulsion from the alpha-phosphate oxygen atoms, the lysine nucleophile stays highly localized, frequently sampling conformations near the electrophile (figures 4A & 4B). The greater frequency is evident in the more concentrated distance-angle distribution, which is reasonably populated for distances less than 3.5Å and angles near 180° (figure 4A). These reactive conformations are made more abundant by the greater fraction of deprotonated lysine-nucleophile expected in the presence of magnesium. Thus, magnesium binding enhances the chances of lysine-intermediate formation. Indeed, it is only when a GTP-bound crystal is soaked in a solution of manganese chloride, providing manganese, a surrogate for magnesium that diffracts X-rays more strongly, that the lysine-GMP intermediate is formed (13).

The computational results reported here strongly imply that magnesium binding activates the lysine nucleophile prior to intermediate formation; however, magnesium induced catalytic enhancement may originate from additional sources, such as transition state stabilization. For example, during associative phosphoryl transfer (16, 17), in which the lysine-nucleophile approaches the electrophile prior to leaving group departure, the reacting phosphate passes through a planar, pentavalent state. This state exhibits a formal negative two or negative three charge, on the phosphate non-bridging oxygen atoms, depending on whether the reaction follows a concerted or addition-elimination pathway, respectively. In each case, the presence of a divalent magnesium cation may provide significant electrostatic stabilization as the pentavalent state forms, which would provide catalytic enhancement by lowering each pathway’s activation barrier. In a dissociative process, on the other hand, the pyrophosphate group departs prior to the lysine nucleophile reacting with the alpha phosphorous electrophile. This results in the departing leaving group accumulating negative charge, which the divalent magnesium cation may also be positioned to stabilize. So, while the exact phosphoryl transfer mechanism is unclear, it is physically reasonable to expect the magnesium ion to participate in some form of transition state stabilization.

While the results reported in this work are specific to the PBCV-1 mRNA capping enzyme, sequence and structural homology to mRNA capping enzymes from other species (44–46),

and to other nucleotidyltransferase superfamily members, allows functional analogies to be drawn that affect our understanding of metal dependence in these enzymes as well. For instance, significant homology among mRNA capping enzymes makes it likely that the magnesium induced lysine activation described in this work is broadly applicable to all mRNA capping enzymes. This is supported, at least in part, by previously reported mutational analysis. D213, which is predicted to coordinate magnesium (figure 4B), is conserved among mRNA capping enzymes from *S. pombe, S. cerevisiae, C. albicans, M. musculus, and H. sapiens* (44) and was found essential during mutational studies of *M. musculus* (44) and *S. cerevisiae* (45) capping enzymes. It is likely that mutating this residue destabilizes magnesium binding, significantly reducing, or completely eliminating magnesium uptake and preventing lysine-GMP intermediate formation. Similarly, structural homology with related nucleotidyltransferase superfamily members implies that magnesium may activate the lysine nucleophile in a manner analogous to that found for the PBCV-1 mRNA capping enzyme. For example, when the ATP-dependent RNA ligase 1 from T4 bacteriophage was crystallized with an unreactive AMPCPP analog, two divalent metals were found in the active site (47). A calcium ion was found adjacent to the alpha-phosphate in a position analogous to the modeled magnesium in this work, while a magnesium ion was coordinated between the beta- and gamma-phosphates (figure 6).

The position of the lysine nucleophiles are very similar in the two structures and, since the two enzymes each form a lysine-nucleoside-monophosphate intermediate and have significantly conserved active site residues, it is plausible that a divalent metal bound at the calcium site activates the lysine nucleophile in a manner identical to that described in this work. Moreover, metal ions have been found, or metal-binding sites proposed, adjacent to the alpha phosphate in other superfamily member active sites (48–50). While these structures correspond to later mechanistic steps, metal reconfiguration is thought to occur following intermediate formation, implying a nucleoside triphosphate metal configuration similar to those in figure 6; consequently, it is likely that the metal ion induced lysine activation described in this work holds across all enzyme types within the superfamily.

Conclusions

Using empirical and thermodynamic integration pK_a estimates, along with conventional MD simulations, we showed how magnesium binding may activate the lysine nucleophile through formation of the lysine-GMP intermediate during the first chemical step of the PBCV-1 mRNA capping enzyme reaction. Consistent with simple electrostatic arguments, both pK_a estimation methods predict that magnesium binding increases lysine nucleophile acidity, enlarging the fraction of the nucleophile in the deprotonated, reactive state. Conventional MD simulations predict that magnesium biases the deprotonated nucleophile to more heavily favor conformations conducive to intermediate formation. While these results increase functional understanding of the *Chlorella* virus capping enzyme, the smallest known functional capping enzyme, homology between capping enzymes across species implies that the results are applicable to all capping enzymes. Similarly, structural and mechanistic homology among members of the nucleotidyltransferase superfamily makes it likely that the magnesium activates the lysine nucleophile of these enzymes as well. While these broader conclusions need to be independently validated on an enzyme-by-enzyme basis, this work provides a platform to understand the magnesium requirements in the PBCV-1 mRNA capping enzyme and possibly other superfamily enzymes.

Supplementary Material

Refer to Web version on PubMed Central for supplementary material.

Acknowledgments

Funding Statement: This work was supported by the NIH Director's New Innovator Award Program 1-DP2-OD007237.

RVS thanks members of the Amaro group for useful discussion during manuscript development.

References

1. Izaurralde E, Lewis J, McGuigan C, Jankowska M, Darzynkiewicz E, Mattaj IW. A nuclear cap binding protein complex involved in pre-mRNA splicing. Cell. 1994; 78:657–668. [PubMed: 8069914]
2. Hamm J, Mattaj IW. Monomethylated cap structures facilitate RNA export from the nucleus. Cell. 1990; 63:109–118. [PubMed: 2208274]
3. Shatkin AJ. mRNA cap binding proteins: essential factors for initiating translation. Cell. 1985; 40:223–224. [PubMed: 3967293]
4. Mao X, Schwer B, Shuman S. Yeast mRNA cap methyltransferase is a 50-kilodalton protein encoded by an essential gene. Mol Cell Biol. 1995; 15:4167–4174. [PubMed: 7623811]
5. Yue Z, Maldonado E, Pillutla R, Cho H, Reinberg D, Shatkin AJ. Mammalian capping enzyme complements mutant Saccharomyces cerevisiae lacking mRNA guanylyltransferase and selectively binds the elongating form of RNA polymerase II. Proc Natl Acad Sci U S A. 1997; 94:12898–12903. [PubMed: 9371772]
6. Tsukamoto T, Shibagaki Y, Imajoh-Ohmi S, Murakoshi T, Suzuki M, Nakamura A, Gotoh H, Mizumoto K. Isolation and characterization of the yeast mRNA capping enzyme beta subunit gene encoding RNA 5′-triphosphatase, which is essential for cell viability. Biochem Biophys Res Commun. 1997; 239:116–122. [PubMed: 9345280]
7. Srinivasan P, Piano F, Shatkin AJ. mRNA capping enzyme requirement for Caenorhabditis elegans viability. J Biol Chem. 2003; 278:14168–14173. [PubMed: 12576475]
8. Shafer B, Chu C, Shatkin AJ. Human mRNA cap methyltransferase: alternative nuclear localization signal motifs ensure nuclear localization required for viability. Mol Cell Biol. 2005; 25:2644–2649. [PubMed: 15767670]
9. Chu C, Shatkin AJ. Apoptosis and autophagy induction in mammalian cells by small interfering RNA knockdown of mRNA capping enzymes. Mol Cell Biol. 2008; 28:5829–5836. [PubMed: 18678651]
10. Shuman S, Lima CD. The polynucleotide ligase and RNA capping enzyme superfamily of covalent nucleotidyltransferases. Curr Opin Struct Biol. 2004; 14:757–764. [PubMed: 15582400]
11. Ho CK, Van Etten JL, Shuman S. Expression and characterization of an RNA capping enzyme encoded by Chlorella virus PBCV-1. J Virol. 1996; 70:6658–6664. [PubMed: 8794301]
12. Venkatesan S, Moss B. Eukaryotic mRNA capping enzyme-guanylate covalent intermediate. Proc Natl Acad Sci U S A. 1982; 79:340–344. [PubMed: 6281766]
13. Hakansson K, Doherty AJ, Shuman S, Wigley DB. X-ray crystallography reveals a large conformational change during guanyl transfer by mRNA capping enzymes. Cell. 1997; 89:545–553. [PubMed: 9160746]
14. Souliere MF, Perreault JP, Bisaillon M. Kinetic and thermodynamic characterization of the RNA guanylyltransferase reaction. Biochemistry. 2008; 47:3863–3874. [PubMed: 18298088]
15. Andreini C, Bertini I, Cavallaro G, Holliday GL, Thornton JM. Metal ions in biological catalysis: from enzyme databases to general principles. J Biol Inorg Chem. 2008; 13:1205–1218. [PubMed: 18604568]
16. Allen KN, Dunaway-Mariano D. Phosphoryl group transfer: evolution of a catalytic scaffold. Trends Biochem Sci. 2004; 29:495–503. [PubMed: 15337123]
17. Fersht, A. Structure and mechanism in protein science : a guide to enzyme catalysis and protein folding. W.H. Freeman; New York: 1999.
18. Li H, Robertson AD, Jensen JH. Very fast empirical prediction and rationalization of protein pKa values. Proteins. 2005; 61:704–721. [PubMed: 16231289]

19. Bas DC, Rogers DM, Jensen JH. Very fast prediction and rationalization of pKa values for protein-ligand complexes. Proteins. 2008; 73:765–783. [PubMed: 18498103]
20. Olsson MHM, Sondergaard CR, Rostkowski M, Jensen JH. PROPKA3: Consistent Treatment of Internal and Surface Residues in Empirical pK(a) Predictions. J Chem Theory Comput. 2011; 7:525–537.
21. Sondergaard CR, Olsson MHM, Rostkowski M, Jensen JH. Improved Treatment of Ligands and Coupling Effects in Empirical Calculation and Rationalization of pKa Values. J Chem Theory Comput. 2011; 7:2284–2295.
22. Tanford C, Roxby R. Interpretation of protein titration curves. Application to lysozyme. Biochemistry. 1972; 11:2192–2198. [PubMed: 5027621]
23. Fersht AR. Conformational equilibria in -and -chymotrypsin. The energetics and importance of the salt bridge. J Mol Biol. 1972; 64:497–509. [PubMed: 5023185]
24. Humphrey W, Dalke A, Schulten K. VMD: Visual molecular dynamics. Journal of Molecular Graphics & Modelling. 1996; 14:33–38.
25. Kirkwood JG. Statistical Mechanics of Fluid Mixtures. Journal of Chemical Physics. 1935; 3:300–313.
26. Frenkel, D.; Smit, B. Understanding Molecular Simulation: From Algorithms to Applications. Academic Press; 2007.
27. Simonson T, Carlsson J, Case DA. Proton binding to proteins: pK(a) calculations with explicit and implicit solvent models. J Am Chem Soc. 2004; 126:4167–4180. [PubMed: 15053606]
28. Xin Y, Hamelberg D. Deciphering the role of glucosamine-6-phosphate in the riboswitch action of glmS ribozyme. Rna. 2010; 16:2455–2463. [PubMed: 20971809]
29. Warshel A, Sussman F, King G. Free energy of charges in solvated proteins: microscopic calculations using a reversible charging process. Biochemistry. 1986; 25:8368–8372. [PubMed: 2435316]
30. Case, DA.; TAD; Cheatham, TE., III; Simmerling, CL.; Wang, J.; Duke, RE.; Luo, R.; Walker, RC.; Zhang, W.; Merz, KM.; Roberts, B.; Hayik, S.; Roitberg, A.; Seabra, G.; Swails, J.; Goetz, AW.; Kolossvai, I.; Wong, KF.; Paesani, F.; Vanicek, J.; Wolf, RM.; Liu, J.; Wu, X.; Brozell, SR.; Steinbrecher, T.; Gohlke, H.; Cai, Q.; Ye, X.; Wang, J.; Hsieh, M-J.; Cui, G.; Roe, DR.; Mathews, DH.; Seetin, MG.; Salomon-Ferrer, R.; Sagui, C.; Babin, V.; Luchko, T.; Gusarov, S.; Kovalenko, A.; Kollman, PA. Amber. 12. University of California; San Francisco: 2012.
31. Wang J, Cieplak P, Kollman PA. How Well Does a Restrained Electrostatic Potential (RESP) Model Perform in Calculating Conformational Energies of Organic and Biological Molecules? J Comput Chem. 2000; 21:1049–1074.
32. Hornak V, Abel R, Okur A, Strockbine B, Roitberg A, Simmerling C. Comparison of multiple Amber force fields and development of improved protein backbone parameters. Proteins. 2006; 65:712–725. [PubMed: 16981200]
33. Meagher KL, Redman LT, Carlson HA. Development of polyphosphate parameters for use with the AMBER force field. J Comput Chem. 2003; 24:1016–1025. [PubMed: 12759902]
34. Oelschlaeger P, Klahn M, Beard WA, Wilson SH, Warshel A. Magnesium-cationic dummy atom molecules enhance representation of DNA polymerase beta in molecular dynamics simulations: improved accuracy in studies of structural features and mutational effects. J Mol Biol. 2007; 366:687–701. [PubMed: 17174326]
35. Jorgensen WL, Chandrasekhar J, Madura JD, Impey RW, Klein ML. Comparison of Simple Potential Functions for Simulating Liquid Water. Journal of Chemical Physics. 1983; 79:926–935.
36. Loncharich RJ, Brooks BR, Pastor RW. Langevin dynamics of peptides: the frictional dependence of isomerization rates of N-acetylalanyl-N′-methylamide. Biopolymers. 1992; 32:523–535. [PubMed: 1515543]
37. Berendsen HJC, Postma JPM, Vangunsteren WF, Dinola A, Haak JR. Molecular-Dynamics with Coupling to an External Bath. Journal of Chemical Physics. 1984; 81:3684–3690.
38. Essmann U, Perera L, Berkowitz ML, Darden T, Lee H, Pedersen LG. A Smooth Particle Mesh Ewald Method. Journal of Chemical Physics. 1995; 103:8577–8593.
39. Morgan BR, Massi F. Accurate Estimates of Free Energy Changes in Charge Mutations. J Chem Theory Comput. 2010; 6:1884–1893.

40. Beutler TC, Mark AE, Vanschaik RC, Gerber PR, Vangunsteren WF. Avoiding Singularities and Numerical Instabilities in Free-Energy Calculations Based on Molecular Simulations. Chem Phys Lett. 1994; 222:529–539.
41. Steinbrecher T, Mobley DL, Case DA. Nonlinear scaling schemes for Lennard-Jones interactions in free energy calculations. Journal of Chemical Physics. 2007; 127
42. Mooney, CZ.; Duval, RD. Bootstrapping: A Nonparameteric Approach to Statistical Inference. Sage; Newbury Park, CA: 1993.
43. Ryckaert JP, Ciccotti G, Berendsen HJC. Numerical-Integration of Cartesian Equations of Motion of a System with Constraints - Molecular-Dynamics of N-Alkanes. J Comput Phys. 1977; 23:327–341.
44. Sawaya R, Shuman S. Mutational analysis of the guanylyltransferase component of Mammalian mRNA capping enzyme. Biochemistry. 2003; 42:8240–8249. [PubMed: 12846573]
45. Wang SP, Deng L, Ho CK, Shuman S. Phylogeny of mRNA capping enzymes. Proc Natl Acad Sci U S A. 1997; 94:9573–9578. [PubMed: 9275164]
46. Chu C, Das K, Tyminski JR, Bauman JD, Guan R, Qiu W, Montelione GT, Arnold E, Shatkin AJ. Structure of the guanylyltransferase domain of human mRNA capping enzyme. Proc Natl Acad Sci U S A. 2011; 108:10104–10108. [PubMed: 21636784]
47. El Omari K, Ren J, Bird LE, Bona MK, Klarmann G, LeGrice SF, Stammers DK. Molecular architecture and ligand recognition determinants for T4 RNA ligase. J Biol Chem. 2006; 281:1573–1579. [PubMed: 16263720]
48. Nandakumar J, Shuman S, Lima CD. RNA ligase structures reveal the basis for RNA specificity and conformational changes that drive ligation forward. Cell. 2006; 127:71–84. [PubMed: 17018278]
49. Odell M, Sriskanda V, Shuman S, Nikolov DB. Crystal structure of eukaryotic DNA ligase-adenylate illuminates the mechanism of nick sensing and strand joining. Mol Cell. 2000; 6:1183–1193. [PubMed: 11106756]
50. Akey D, Martins A, Aniukwu J, Glickman MS, Shuman S, Berger JM. Crystal structure and nonhomologous end-joining function of the ligase component of Mycobacterium DNA ligase D. J Biol Chem. 2006; 281:13412–13423. [PubMed: 16476729]

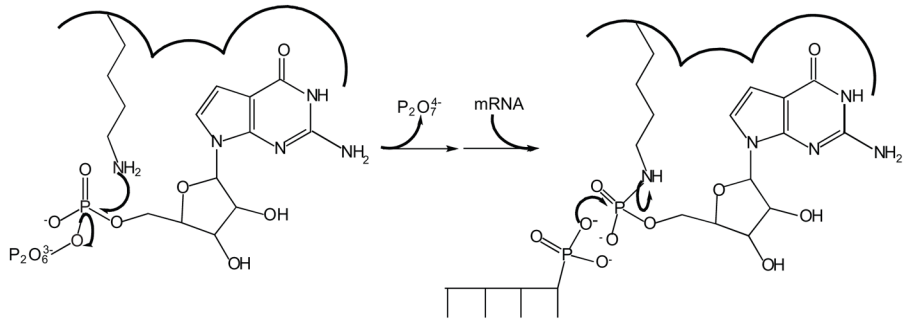

Figure 1.

Guanylyltransferase mRNA capping mechanism. Following GTP binding, a conserved lysine nucleophile attacks the alpha-phosphorous atom of GTP, displacing pyrophosphate, resulting in the formation of a lysine-GMP intermediate. After the release of pyrophosphate and the subsequent binding of nascent mRNA, GMP is transferred from the lysine nucleophile to the mRNA 5′-phosphate completing the reaction

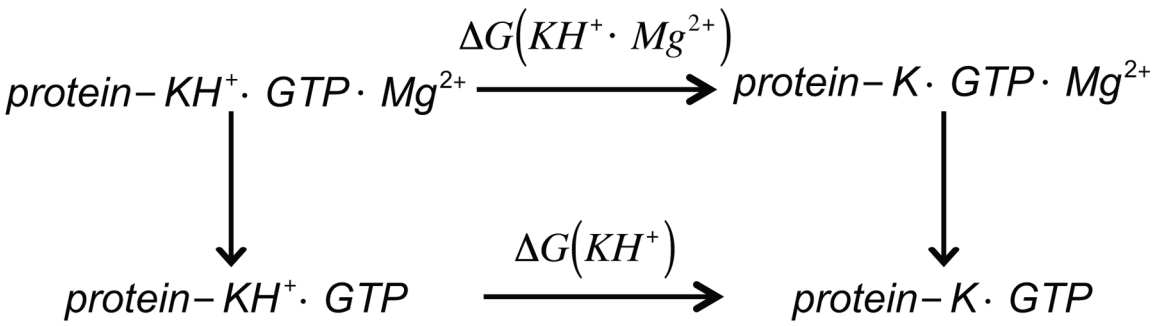

Figure 2.
Thermodynamic cycle linking lysine nucleophile deprotonation in the presence and absence of magnesium bound in the active site.

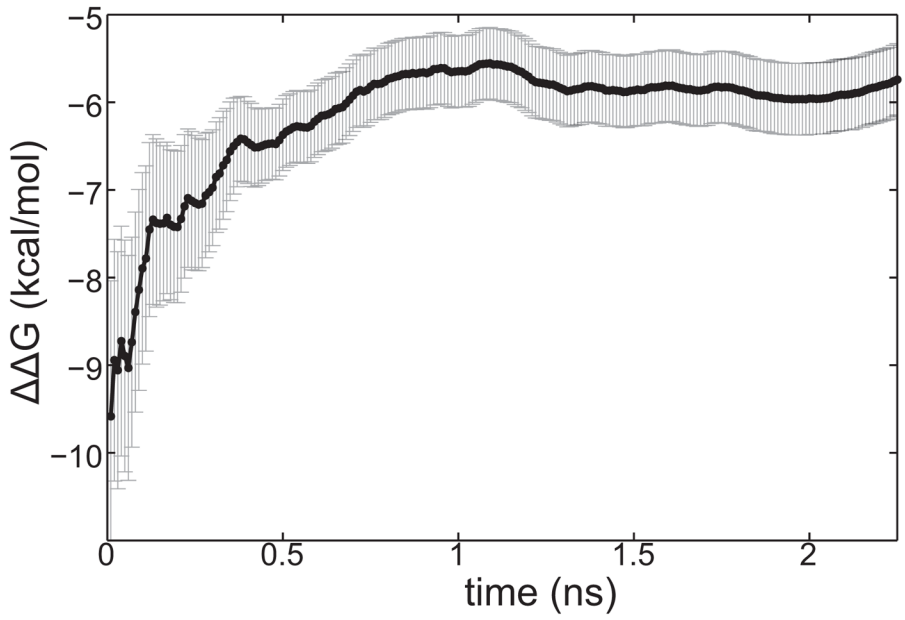

Figure 3.

Double free energy change ($\Delta\Delta G$) time series. $\Delta\Delta G$ was determined by subtracting the change in free energy of deprotonating the lysine nucleophile GTP-bound state from the change in free energy of deprotonating the lysine nucleophile in the GTP-magnesium-bound state and is described in figure 2. Standard error is reported.

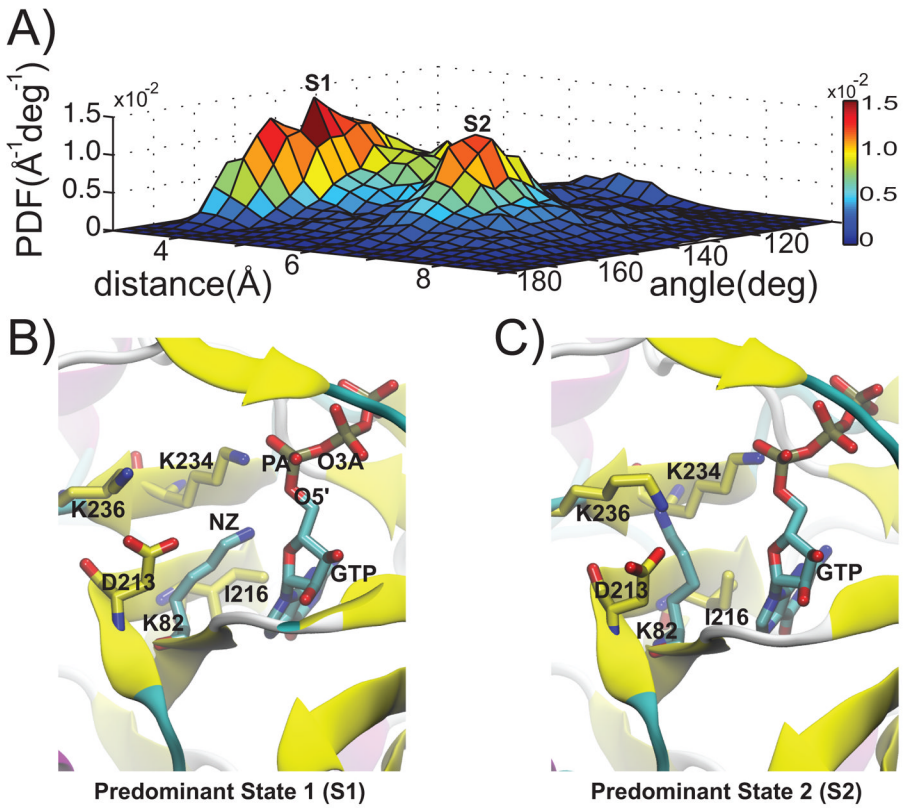

Figure 4.

Magnesium unbound active-site geometry. A) Two-dimensional probability distribution function (PDF) showing two predominant states, S1 and S2: “distance” marks the separation of the NZ nitrogen-nucleophile atom of K82 and the PA phosphorus-electrophile atom of GTP; “angle” indicates the angle formed by the NZ nucleophile, the PA electrophile, and the O3A oxygen atom, the first atom of the pyrophosphate leaving group. Each of these atoms is labeled in figure 4B. B) A representative conformation from the predominant state with the smaller nucleophile-electrophile separation, S1. C) A representative conformation from the predominant state with the larger nucleophile-electrophile separation, S2. In both B) and C) a pocket formed by K236, K234, D213, and I216 is shown with yellow carbon atoms, while K82 and GTP carbon atoms are colored cyan.

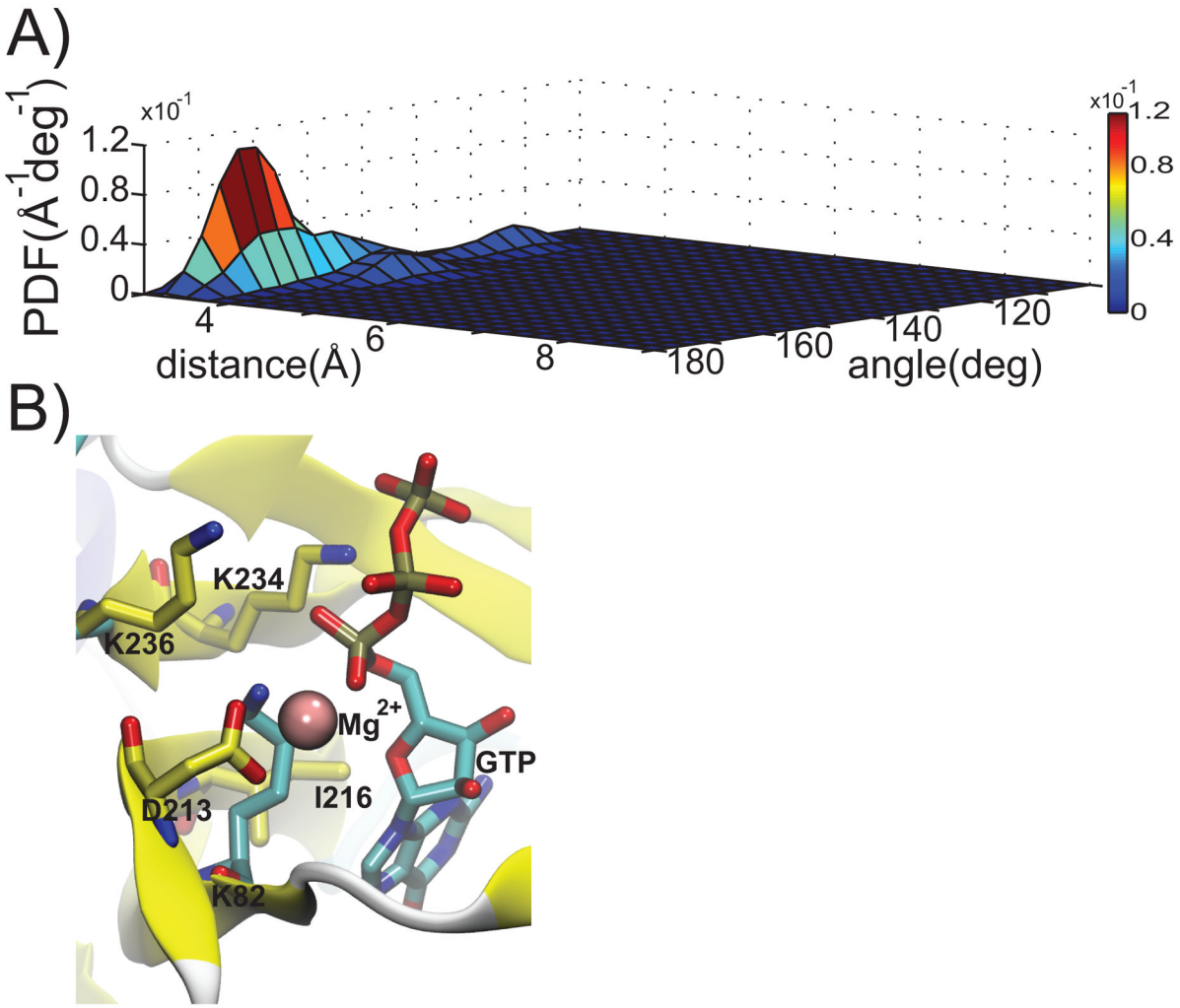

Figure 5.

Magnesium bound active-site geometry. A) Two-dimensional probability distribution function (PDF) showing one predominant state: “distance” and angle are as defined in figure 3A. B) A representative conformation from the predominant state. Magnesium is shown as a magenta sphere. For reference, K236, K234, D213, and I216 are shown in yellow. K82 and GTP carbon atoms are shown in cyan.

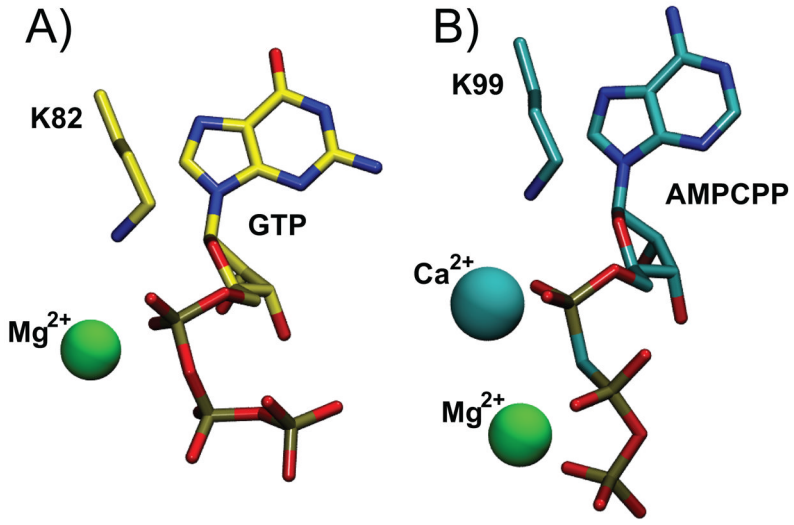

Figure 6.

Metal position homology among nucleotidyltransferase superfamily members. A) The PBCV-1 mRNA capping enzyme showing the position of the modeled magnesium ion, the lysine nucleophile and GTP. Carbon atoms are colored yellow. B) The T4-phage RNA ligase showing the position of co-crystallized calcium and magnesium ions, the lysine nucleophile, and an unreactive ATP analog, AMPCPP. Carbon atoms are shown in cyan.

Table 1

Comparing pK_a prediction methods[a]

Method	pK_a without Mg^{2+}	pK_a with Mg^{2+}	ΔpK_a
PROPKA	14.51	7.89	− 6.6
TI	-	-	− 4.2+/−0.3

[a]For the PROPKA results, ΔpK_a was determined by subtracting the value without Mg^{2+} from the value with Mg^{2+}. PROPKA is deterministic and yields a single value for a single structure, so no statistical error is reported. For the TI results, ΔpK_a was determined using equation 3 and error calculated with standard propagation techniques.